Effect of Proton Radiation on Ultrawide Bandgap AlN Schottky Barrier Diodes

Jossue Montes, Tsung-Han Yang, Houqiang Fu, Hong Chen, Xuanqi Huang, Kai Fu, Izak Baranowski, and Yuji Zhao

***Abstract*— Lateral Pd/n-AlN Schottky barrier diodes (SBDs) were fabricated and subjected to 3-MeV proton irradiation at various fluences. Electrical and material characterization analysis was performed before and after each radiation fluence to quantify the change in device characteristics. It was found that the SBDs performed reliably up to a proton irradiation fluence of 5×10^{13} cm^{-2}, with little or no change in the key device performance, such as current, turn-on voltage, ideality factor, breakdown voltage, and so on. The electrical characteristics of the SBDs were well-predicted using a standard thermionic emission theory. The performance of the SBDs shows a significant degradation after a high-fluence irritation of 5×10^{15} cm^{-2}, where the current of the SBDs dropped two orders in magnitude. Material and surface characterizations, including atomic force microscopy and X-ray diffraction, indicated a consistent degradation in the AlN bulk crystal quality and a drastic increase in surface roughness. These results provide valuable information on the radiation properties of AlN electronics and can serve as important references for the future development of high-performance AlN devices for extreme environment applications.**

***Index Terms*— Aluminum nitride, barrier height, breakdown voltage, ideality factor, leakage current, radiation effects, Schottky barrier diodes (SBDs), surface roughness, turn-on voltage.**

I. Introduction

THE radiation hardness of a semiconductor is a critical material quality for the design and fabrication of radiation-insensitive semiconductor electronic devices and systems for various extreme environments such as space missions, advanced military operations, and nuclear power stations [1]. GaN-based wide bandgap (WBG) semiconductor devices such as AlGaN/GaN high-electron mobility transistors, PIN diodes, and light-emitting devices have been extensively studied due to their high-radiation performance [2]–[5]. Recently, the ultra-WBG (UWBG) semiconductor AlN, which has a bandgap ($E_g \sim 6.2$ eV) significantly larger than GaN ($E_g \sim 3.4$ eV), has emerged as an attractive material candidate for next-generation radiation-insensitive power and RF electronic applications [6]. Their advantageous material properties include a WBG of 6.2 eV, a tough chemical bonding rated at 11.52 eV/atom, a high-electron mobility of 1090 cm^2/V · s, a high-critical field (E_c) of 12 mV/cm, and a high maximum operating temperature of 690 °C [7]. Since the radiation tolerance nonlinearly scales with the bandgaps of the materials, superior radiation hardness can also be expected from UWBG AlN [8], [9]. Despite the high-potential AlN, there are currently a very few reports in the literature that discuss the radiation effects in AlN materials and devices mainly due to the challenges in producing high-quality AlN crystals and reliable AlN devices [6].

Recent years have seen very successful demonstrations of growing AlN on low-cost sapphire substrates, partially mitigating the cost and performance setbacks [10]–[13]. In this paper, we present the first report of the proton radiation experiment on AlN Schottky barrier diodes (SBDs). AlN SBDs were grown and fabricated via metal organic chemical vapor deposition (MOCVD) and subjected to proton irradiation using 3-MeV protons at four different fluxes: 5×10^9 cm^{-2}, 5×10^{11} cm^{-2}, 5×10^{13} cm^{-2}, and 5×10^{15} cm^{-2}. Material and electrical characterizations were performed after each fluence to examine the radiation effects on AlN materials and SBD devices. The results showed that the AlN SBDs maintain a consistent performance until a high-proton fluence of 5×10^{15} cm^{-2}, where significant degradations in device characteristics, crystal quality, and surface roughness were observed.

II. Growth and Fabrication

MOCVD was used to grow AlN epilayers on a single-side polished (0001) sapphire substrate. The epilayers consisted of an AlN buffer layer followed by a 1-μm thick unintentionally doped AlN resistive layer and a 300-nm n-AlN layer. The precursor gases used in the MOCVD reactor were trimethylaluminum (TMAl) and ammonia (NH_3), which supplied the Al and N elements, and silane (SiH_4), which supplied Si for n-type doping. A 2-nm GaN capping layer was employed on the top portion of the n-AlN layer to prevent oxidation of the surface [14]. The crystal quality of the grown-up AlN epilayers was examined using high-resolution X-ray diffraction (HR-XRD). The full-width at half-maximum (FWHM) value was found to be 0.013° for the 0002 plane and 0.044° for the $20\bar{2}4$ plane. Further information can be found in [15].

Manuscript received July 29, 2018; revised September 28, 2018, November 5, 2018, and November 9, 2018; accepted November 20, 2018. Date of publication November 30, 2018; date of current version January 17, 2019. This work was supported by DTRA YIP under Grant HDTRA11710041.

The authors are with the School of Electrical, Computer, and Energy Engineering, Arizona State University, Tempe, AZ 85287 USA (e-mail: yuji.zhao@asu.edu).

Color versions of one or more of the figures in this paper are available online at http://ieeexplore.ieee.org.

Digital Object Identifier 10.1109/TNS.2018.2883400

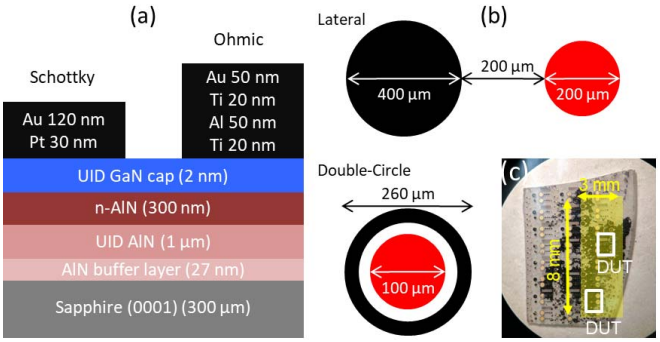

Fig. 1. Design and fabrication of the AlN SBDs. (a) Device schematic. (b) Top-down view of two devices: the double-circle SBD and the normal lateral SBD including an image of the fabricated AlN sample. (c) Finished sample. The proton beam spot size and devices under test are indicated in yellow and white, respectively.

The AlN sample was cleaned under ultrasonic agitation using acetone for 5 min followed by an additional 5 min using isopropyl alcohol. Standard photolithography using photoresist (3312 and LOR3A) was used to pattern and expose the contacts. Prior to metal deposition, the sample was cleaned in a 1:2 mixture of HCl:H_2O. The ohmic contact stack consisted of Ti/Al/Ti/Au (20/100/20/50 nm). After the ohmic contact deposition, the sample was annealed at 1000 °C in N_2 for 30 s. The Schottky contact stacks were Pt/Au (30/120 nm). The SBDs consisted of circular ohmic and Schottky contacts. There were two kinds of devices: lateral SBDs and double-circle SBDs. For the lateral SBDs, the ohmic and Schottky contacts were 400 and 200 μm in diameter, respectively. The lateral separation distance between the two contacts is 200 μm. For the double-circle SBDs, the diameter of the ohmic and Schottky contacts is 260 and 100 μm, respectively. Fig. 1 shows the schematic device structures of the AlN SBDs and the top-down views of the double-circle and the lateral SBDs as well as an image of the fully fabricated AlN sample. The finished sample hosts approximately 312 SBDs. A full explanation of various SBD geometries designed and implemented can be found in [16].

The crystal qualities of the AlN were examined by the HR-XRD scans using a Panalytical X'Pert Pro X-ray diffractometer. The setup used Cu Kα radiation along with a hybrid monochromator (for incident beam optics) and triple axis module (diffracted). The surface morphologies of the AlN samples were examined by the use of atomic force microscopy (AFM) scans. The device characteristics of the AlN SBDs, such as current–voltage (I–V) and capacitance–voltage (C–V) characteristics, were analyzed using a Keithley 4200-SCS parameter analyzer with a sample held on a thermally controllable stage. The I–V characteristics were studied across a temperature range from 20 °C to 120 °C, while the C–V characteristics were done at room temperature. After the initial set of characterizations, the SBDs were bombarded with 3-MeV protons at four fluxes ranging from 5×10^9 cm^{-2} to 5×10^{15} cm^{-2} at 300 K at ASU's iBeAM facility. This range is similar to the ranges used in similar radiation studies on GaN [4], [5]. The incident proton beam is rectangular, approximately 3×8 mm^2 in size, which allows approximately half the sample to be bombarded. Characterization tests were repeated after each fluence to study the impact of radiation on AlN materials and device characteristics. The intensity of the beam decays rapidly outside this region.

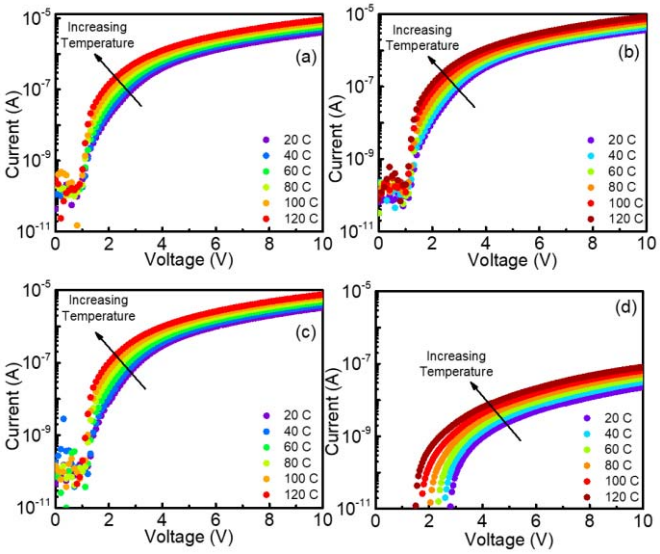

Fig. 2. Forward-bias I–V characteristics from 20 to 120 °C for the AlN SBDs under various proton irradiation fluences: (a) No radiation, (b) 5×10^9 cm^{-2}, (c) 5×10^{13} cm^{-2}, and (d) 5×10^{15} cm^{-2}.

III. Results and Discussion

A standard thermionic emission model was used to model the AlN SBDs, which is given as [17], [18]

$$J = J_0 \left(\exp\left(\frac{q(V - IR_S)}{nk_BT} \right) - 1 \right) \quad (1)$$

$$J_0 = A^* T^2 \exp\left(-\frac{\Phi_B}{k_BT} \right) \quad (2)$$

where J is the current density, q is the electronic charge, R_S is the series resistance, n is the ideality factor, J_0 is the saturation current density, A^* is the Richardson constant, T is the temperature, Φ_B is the Schottky barrier height (SBH), and k_B is the Boltzmann constant. For our AlN SBDs, the Richardson constant is equal to 48 A cm$^{-2} \cdot$ K^{-2}.

Fig. 2 shows the forward-bias I–V characteristics of the AlN SBDs under different proton irradiation fluence. The SBDs perform consistently and reliably up to the fluence of 5×10^{13} cm^{-2}. After the highest proton fluence of 5×10^{15} cm^{-2}, the current of the SBDs drops by two orders of magnitude.

Fig. 3 represents the turn-on voltage versus temperature for the AlN SBDs under different proton irradiation fluences. The turn-on voltage is simply determined as the voltage at which significant current begins to flow. At every radiation fluence level, the turn-on voltage decreases with increasing temperature, dropping on average of 0.2 V across the temperature range studied. At the highest radiation fluence (5×10^{15} cm^{-2}), the drop of the turn-on voltage is approximately 1.35 V. This curve is included as an inset because of the drop in current magnitudes [see Fig. 2(d)], and turn-on voltage is determined independently from the first four curves. However, the inverse relationship with temperature is still present in the 5×10^{15} cm^{-2} case. The ideality factor n and SBH Φ_B

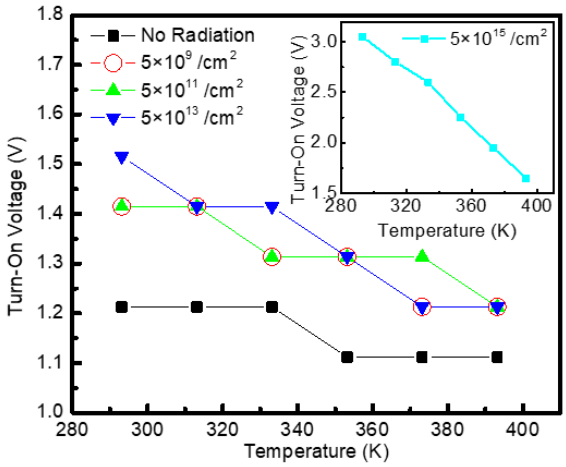

Fig. 3. Turn-on voltages versus temperatures for the AlN SBDs under different proton irradiation fluence. Inset: turn-on voltage after the 5×10^{15} cm^{-2}, which was calculated independently from the other fluences due to the large difference in diode current magnitudes.

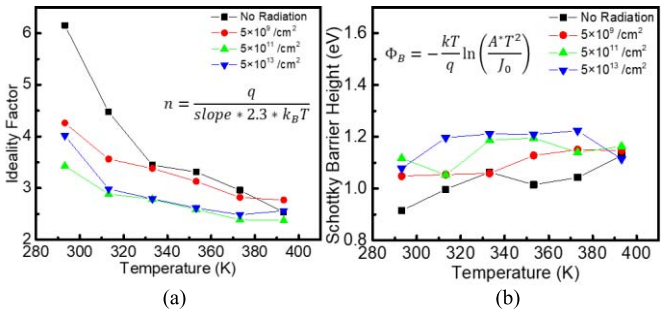

Fig. 4. (a) Ideality factor and (b) SBH versus temperatures for the AlN SBDs under different proton irradiation fluences.

can be extracted from (1) and (2), represented in Fig. 4. The ideality factors decrease with increasing temperature and decrease with increasing radiation fluence. The SBH generally increases slightly with increasing temperature and increasing radiation fluence. The behavior of the ideality factor and SBH with regard to temperature is a well-known phenomenon for many common diodes and is a result of contact-substrate inhomogeneity.

Fig. 5 shows the reverse-bias I–V characteristics of the AlN SBDs under various proton irradiation fluence. As predicted by the thermionic emission model, the current magnitudes of the AlN SBDs increase with increasing temperatures. Up to the fluence of 5×10^{13} cm^{-2}, the current magnitudes of the SBDs are difficult to distinguish from one another, indicating that the AlN SBDs are resisting radiation-induced degradation at least up to this flux. After the largest fluence of 5×10^{13} cm^{-2}, the currents have decreased by three orders of magnitude.

Fig. 6 shows the breakdown voltage (V_{BR}) versus temperature for the AlN SBDs under various proton irradiation fluences. Similar to turn-on voltage, the breakdown voltage is the voltage at which significant reverse-bias current begins to flow. The magnitude and the temperature dependence of V_{BR} are nearly unchanged throughout the first three radiation fluences. After the 5×10^{13} cm^{-2} fluence, the breakdown voltage drops approximately 4 V. The average decrease for the first three fluences is 5.6 V. Owing to the sharp drop in reverse-bias current magnitudes that occur between the 5×10^{13} cm^{-2}

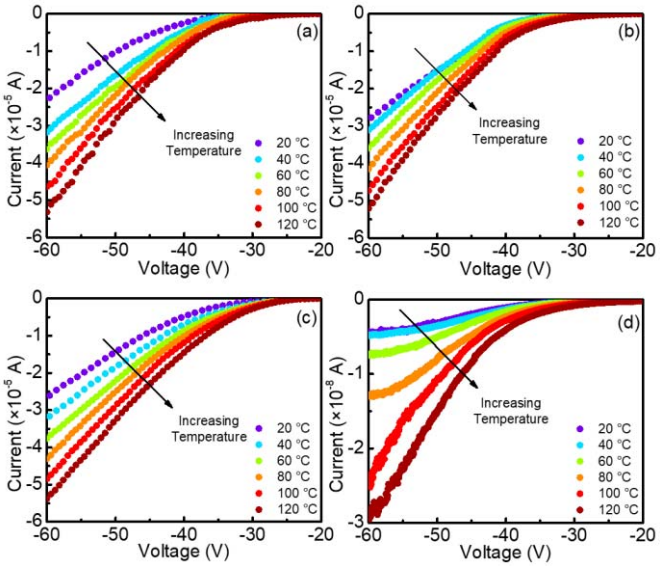

Fig. 5. Reverse-bias current from 20 °C to 120 °C for the 3-MeV proton irradiation fluences (a) 5×10^{9} cm^{-2}, (b) 5×10^{11} cm^{-2}, (c) 5×10^{13} cm^{-2}, and (d) 5×10^{15} cm^{-2}. The currents in (d) have decreased by three orders of magnitude compared with the other figures.

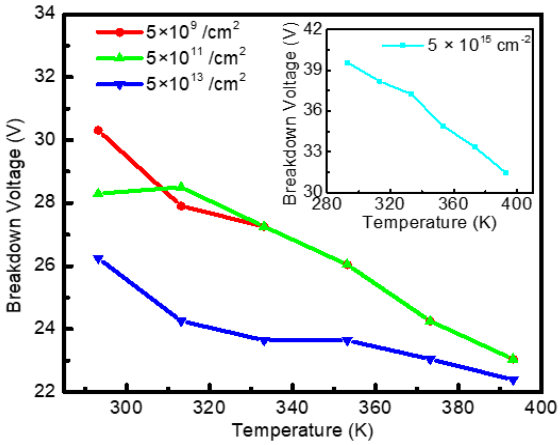

Fig. 6. Reverse-bias breakdown voltage versus temperatures for the AlN SBDs under various proton irradiation fluences. Inset: breakdown voltage for after the highest radiation fluence (5×10^{15} cm^{-2}), determined independently from the other three fluences.

and 5×10^{15} cm^{-2} fluence, the breakdown voltage was independently determined for the 5×10^{15} cm^{-2} fluence, and it can be seen in the inset of Fig. 6. Furthermore, we can see that in all the cases, the breakdown voltage has a negative dependence on temperature. This behavior is consistent with a breakdown mechanism related to surface states [19]. It is well-established that surface states on AlN arise due to Al dangling bonds [20], [21]; also, AlN has a very large density of surface states, larger than that of other materials including GaN-based devices [22]. Due to the large presence of surface states, it is likely that they contribute significantly to device breakdown [23], [24].

Fig. 7 represents the reverse-bias leakage currents at two different biases (−20 and −50 V) as functions of temperature of the AlN SBDs under different proton irradiation fluences. The leakage currents are not strongly affected by increasing radiation up to the 5×10^{13} cm^{-2} fluence. At −20 V, the leakage currents are the strong function of temperature, but as we

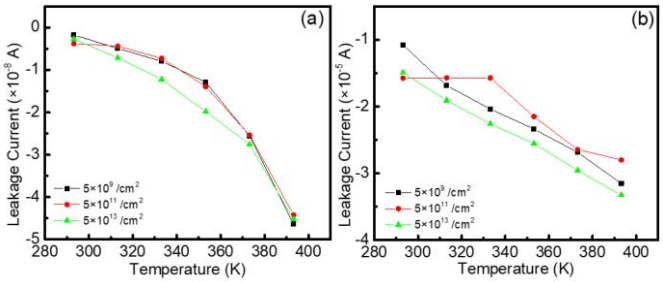

Fig. 7. Reverse-bias leakage currents versus temperatures for the AlN SBDs under various proton irradiation fluences for (a) −20 V and (b) −50 V.

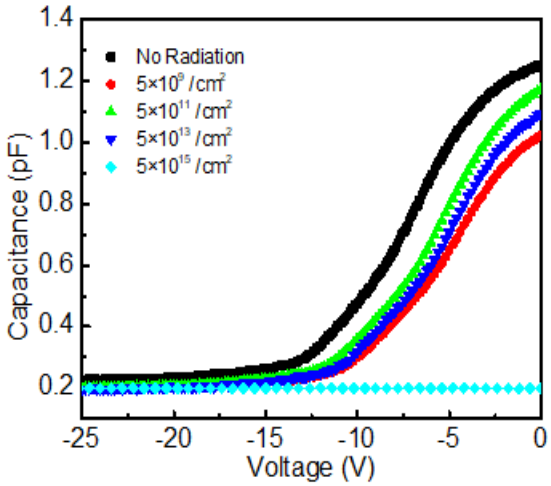

Fig. 8. C–V characteristics for the various proton radiation fluences.

move to −50 V, the temperature dependence becomes linear. As can be seen, there is close to zero change in reverse-bias leakage current with increasing radiation fluence.

Fig. 8 shows the C–V characteristics of the AlN SBDs under various proton irradiation fluences. The C–V characteristics remain relatively unchanged up to the proton fluence of 5×10^{13} cm^{-2}. After the fluence of 5×10^{15} cm^{-2}, the C–V curve of the SBDs collapses. The effective carrier concentration can be approximated using the following [25], [26]:

$$C^{-2} = \frac{2}{q\varepsilon_0\varepsilon_r N_D}\left(V_{\text{bi}} - V - \frac{kt}{q}\right) \tag{3}$$

$$\frac{d(C^{-2})}{dV} = -\frac{2}{q\varepsilon_0\varepsilon_r N_D} \tag{4}$$

where V_{bi} is the built-in voltage, ε_0 is the vacuum permittivity (8.84×10^{-14} F·cm^{-1}), ε_r is the AlN permittivity (10.1), and N_D is the n-type carrier concentration. By plotting the derivative of $1/C^2$ against the applied voltage using (4), the *effective* carrier concentration can be obtained. [The plot is actually $(\text{Area}/C)^2$ versus V, where Area is the area of the Schottky contact of the SBD in centimeters. The SBDs used for C–V measurements are exclusively of the double-circle design, and the Schottky contact has a diameter of 260 μm.] The effective carrier concentration calculated in the n-AlN layer using (4) is around 10^{14} cm^{-3} and does not deviate up to the proton fluence of 5×10^{13} cm^{-2}. After the fluence of 5×10^{15} cm^{-2}, the effective carrier concentration cannot be reliably approximated.

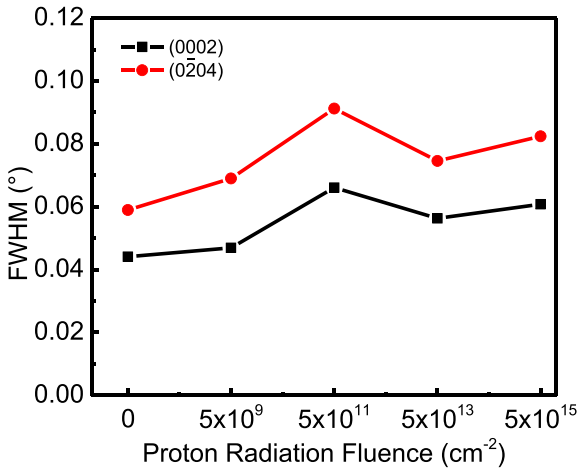

Fig. 9. HR-XRD FWHM values for the AlN SBDs as functions of proton radiation fluence.

The HR-XRD scans were used to determine the crystal quality change as a function of radiation fluence. The FWHM values quantify the quality of the crystal planes; smaller FWHM values indicate higher crystal quality. These values are represented in Fig. 9. The FWHM values can be seen rising after each radiation fluence in a consistent trend. This indicates a degradation in the crystal quality with each radiation fluence. The slight increase after the 10^{11} cm^{-2} fluence can be attributed to small differences in the experimental setup.

In order to characterize the surface topography of the bombarded regions in the AlN SBDs, the AFM scans were carried out using a Bruker Multimode 8 in tapping mode. Fig. 10 shows, the AFM scans after the highest fluence in two distinct regions: (1) is a region far away from the irradiated SBDs and (2) is a region directly under the full intensity of irradiation. Of the 47 scans, it was found that region (1) had an average surface roughness of 7.68 nm and region (2) had 16.03 nm. In region (2), it is clearly visible, a number of particulates/surface abnormalities that the AFM scans reveal to be between 50 and 150 nm in height on average. These "nano needles" are a ubiquitous finding in the irradiated region, but so far less in the unirradiated region [region (1)]. Furthermore, where they do occur in region (1), their heights are typically much lower, rarely venturing taller than 50 nm. The 3-D AFM scan of region (2) is shown in Fig. 10(b). The exact mechanism responsible for the formation is a topic of current investigation.

A Hitachi S4700 field emission scanning electron microscope was used to perform energy dispersive X-ray spectroscopy on the sample in order to probe the elemental character of the surface particulates in region (2), and the results are shown in Fig. 11. The Al and N peaks are visibly evident; however, the N peak is much smaller than the Al peak. This is possibly due to the experimental setup prior to the SEM imaging; and 10 nm of Au was deposited on the sample to help in SEM imaging. Such a thickness would make energy dispersive X-ray data-collecting difficult because the Au atoms absorb much of the incoming energy, making it difficult to get a signal from other atoms such as N. In fact, the Au peak (not shown in Fig. 11) is always comparable to the Al peak. The Ga signal is likely from the GaN capping layer; another potential source is Ga contamination in the MOCVD chamber,

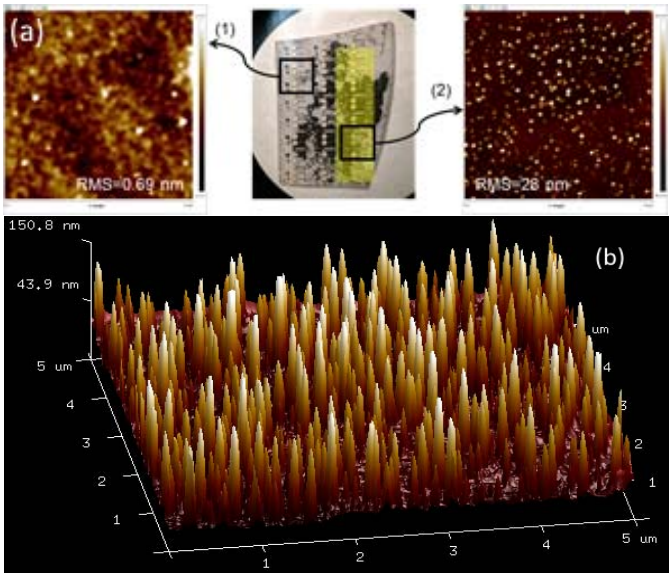

Fig. 10. (a) AFM images in two distinct regions: (1) is a region far away from the proton bombardment and (2) is directly under the full intensity of the beam. (b) 3-D AFM image in region (2) showing the height of the surface features.

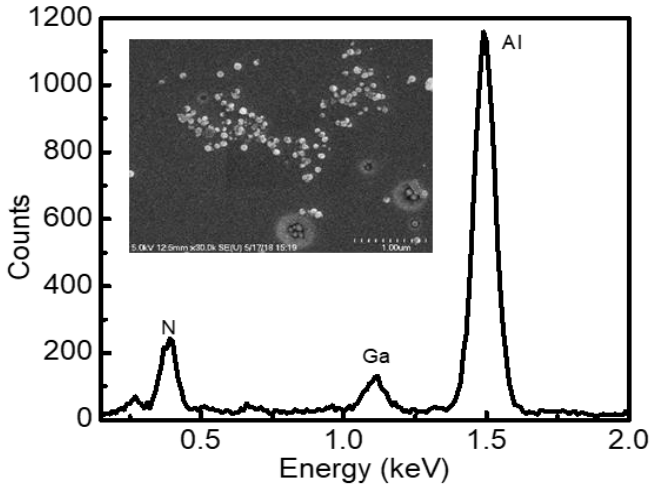

Fig. 11. EDX spectrum from the SEM image (inset), taken in region 2 (the region irradiated by protons). The prominent Au peak is omitted.

which is a common issue. No other elemental peaks are evident in any of the scans performed, indicating that the surface particulates are probably a radiation-induced deformation of the AlN crystal.

Because of their charge and mass, protons in general cause damage to a material by direct ionization, where orbital electrons are removed from atoms in the target, and lattice displacement, where atoms are physically knocked out from the crystal lattice. The software package stopping and range of ions in matter (SRIM) was used to estimate the amount of damage by modeling the interaction between the incident protons and the AlN SBDs. By recreating the 300-nm n-AlN layer being hit with 3-MeV protons at normal incidence in SRIM, the n-AlN layer is completely and easily penetrated, with little branching or spreading away from the normal direction [see Fig. 12(a)]. The SRIM estimates a peak population of protons occurring at 61.36 μm, well into the 300-μm sapphire layer. This indicates that the 3-MeV protons are quite easily

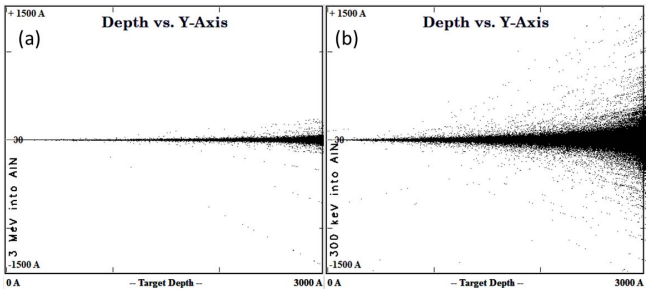

Fig. 12. SRIM model for the 300-nm n-AlN layer with 3-MeV incident protons. (a) 3-MeV protons. (b) 300-keV protons.

penetrating through the conductive layer of the AlN SBDs. The SRIM approximates that in the n-AlN layer, 99.93% of the energy loss is given as ionization, with the rest going toward phonons and recoils (secondary collisions). There is 0% energy lost while creating lattice vacancies. For comparison, reducing the proton energies to 300 keV results in a penetration depth of 2.02 μm, again with nearly all the energy (99.88%) being lost as ionization. However, at this energy level, the protons spread out significantly more in the n-AlN layer [Fig. 12(b)].

It has been observed that annealing of materials after irradiation can potentially recover some of the damage done. The thermal stability of radiation defects is a measure of how resilient the defects would be against thermal annealing. Similar studies [27] on GaN devices have remarked on the thermal stability of defects and their resistance to annealing recovery. Gallium interstitial defects (which act as donors) have been observed to anneal at room temperature conditions, while gallium vacancies have shown stability up to 500 °C [28]. Temperature as low as 150 °C was needed to begin improving the sheet resistivity of an undoped GaN sample after irradiated with fast and thermal neutrons at a fluence of 1.5×10^{17} cm^{-2} [29].

While none of the SBDs in this paper were annealed in a controlled setting (under vacuum with select gases) after irradiation, there is a possibility that the thermal stage used during testing would have an annealing effect even in an open air setting. In this paper, the thermal chuck was run-up to 140 °C with the sample in place. These are similar conditions to those used by Karmarkar *et al.* [30], where a complete restoration of diode ideality factor and series resistance was observed in GaN SBDs after annealing in air at a temperature of 250 °C. In [30], 1-MeV protons were used. In this paper, the SBD ideality factors show a slight improvement as temperature increases. In the case of no radiation, the ideality factor decreases by 3.6, and in the 5×10^{9} cm^{-2}, 5×10^{11} cm^{-2}, and 5×10^{13} cm^{-2} fluences, the drops are 1.5, 1.1, and 1.5, respectively. These values are comparable to the study as mentioned earlier. One method to determine the extent to which radiation defects were recovered would be to use deep level transient spectroscopy, which could help to see the energy levels and impact of the defects.

IV. Conclusion

Lateral Pd/n-AlN SBDs were fabricated by the MOCVD and subjected to 3-MeV proton irradiation at various fluxes. Based upon the findings of forward- and reverse-biased

I–V measurements and C–V characteristics, the electrical performance of the devices was not reasonably impacted up to the fluence of 5×10^{13} cm^{-2}. Diode turn-on voltages increase with increasing radiation fluence and their rate of decrease with increasing temperature is greater at higher radiation fluences. Diode ideality factors consistently decrease with increasing temperature and decrease with increasing radiation fluence. The SBHs increase with increasing radiation fluence and temperature. Breakdown voltage decreases with increasing temperature and remains resilient with regard to increasing radiation fluence. C–V characteristics show a consistent character up to the 5×10^{13} cm^{-2} fluence. After the highest proton irradiation fluence of 5×10^{15} cm^{-2}, the current of the AlN SBDs decreased by two orders of magnitude, and some measurements become difficult or impossible to interpret (e.g., C–V data). The HR-XRD scans reveal a consistent increase in FWHM values in the AlN crystal with increasing proton irradiation fluence, indicating a degradation in the bulk crystal with proton bombardment. AFM scans show increased surface roughness in the region bombarded with protons compared to the region not bombarded. In addition, AFM scans reveal the presence of "nano needles" in the bombarded region, with heights exceeding 100 nm.

Acknowledgment

The authors would like to thank the LeRoy Eyring Center for Solid State Science, Arizona State University.

References

[1] P. J. Sellin and J. Vaitkus, "New materials for radiation hard semiconductor dectectors," *Nucl. Instrum. Methods Phys. Res. A,Accel. Spectrom. Detect. Assoc. Equip.*, vol. 557, no. 2, pp. 479–489, Feb. 2006, doi: 10.1016/j.nima.2005.10.128.

[2] S. J. Pearton, Y.-S. Hwang, and F. Ren, "Radiation effects in GaN-based high electron mobility transistors," *JOM*, vol. 67, no. 7, pp. 1601–1611, Jul. 2015.

[3] L. Lv *et al.*, "Fast and thermal neutron radiation effects on GaN PIN diodes," *IEEE Trans. Nucl. Sci.*, vol. 64, no. 1, pp. 643–647, Jan. 2017, doi: 10.1109/TNS.2016.2630061.

[4] C.-H. Lin *et al.*, "Neutron irradiation effects on gallium nitride-based Schottky diodes," *Appl. Phys. Lett.*, vol. 103, no. 16, Oct. 2013, Art. no. 162106, doi: 10.1063/1.4826091.

[5] A. Y. Polyakov, S. J. Pearton, P. Frenzer, F. Ren, L. Liu, and J. Kim, "Radiation effects in GaN materials and devices," *J. Mater. Chem. C*, vol. 1, no. 5, pp. 877–887, 2013, doi: 10.1039/c2tc00039c.

[6] J. Y. Tsao *et al.*, "Ultrawide-bandgap semiconductors: Research opportunities and challenges," *Adv. Electron. Mater.*, vol. 4, no. 1, Dec. 2017, Art. no. 1600501, doi: 10.1002/aelm.201600501.

[7] E. Schubert. (Jul. 20, 2018). *Educational Resources*. [Online]. Available: http://www.ecse.rpi.edu/schubert/Educational-resources/Educational-resources.htm

[8] L. Trinkler, B. Berzina, A. Auzina, M. Benabdesselam, and P. Iacconi, "Use of aluminum nitride for UV radiation dosimetry," *Nucl. Instrum. Methods Phys. Res. A, Accel. Spectrom. Detect. Assoc. Equip.*, vol. 580, no. 1, pp. 354–357, Sep. 2007, doi: 10.1016/j.nima.2007.05.177.

[9] B. Reinhard, B. R. Tittmann, and A. Suprock, "Nuclear radiation tolerance of single crystal aluminum nitride ultrasonic transducer," *Phys. Procedia*, vol. 70, pp. 609–613, Sep. 2015, doi: 10.1016/j.phpro.2015.08.036.

[10] Y. A. Xi *et al.*, "Very high quality AlN grown on (0001) sapphire by metal-organic vapor phase epitaxy," *Appl. Phys. Lett.*, vol. 89, no. 10, p. 103106, Sep. 2006, doi: 10.1063/1.2345256.

[11] T. Y. Wang, J. H. Liang, G. W. Fu, and D. S. Wuu, "Defect annihilation mechanism of AlN buffer structures with alternating high and low V/III ratios grown by MOCVD," *CrystEngComm*, vol. 18, no. 47, pp. 9152–9159, Nov. 2016, doi: 10.1039/C6CE02130A.

[12] A. Knauer *et al.*, "Correlation of sapphire off-cut and reduction of defect density in MOVPE grown AlN," *Phys. Status Solidi B*, vol. 253, no. 5, pp. 809–813, Mar. 2016, doi: 10.1002/pssb.201600075.

[13] Y. Irokawa, E. A. G. Víllora, and K. Shimamura, "Shottky barrier diodes on AlN free-standing substrates," *Jpn. J. Appl. Phys.*, vol. 51, no. 4R, p. 040206, Mar. 2012, doi: 10.1143/JJAP.51.040206.

[14] G. Li *et al.*, "Two-dimensional electron gases in strained quantum wells for AlN/GaN/AlN double heterostructure field-effect transistors on AlN," *Appl. Phys. Lett.*, vol. 104, no. 19, p. 193506, May 2014, doi: 10.1063/1.4875916.

[15] H. Fu *et al.*, "Demonstration of AlN Schottky barrier diodes with blocking voltage over 1 kV," *IEEE Electron Device Lett.*, vol. 38, no. 9, pp. 1286–1289, Sep. 2017, doi: 10.1109/LED.2017.2723603.

[16] H. Fu, X. Huang, H. Chen, Z. Lu, and Y. Zhao, "Fabrication and characterization of ultra-wide bandgap AlN-based Schottky diodes on sapphire by MOCVD," *IEEE J. Electron Devices Soc.*, vol. 5, no. 6, pp. 518–524, Nov. 2017, doi: 10.1109/JEDS.2017.2751554.

[17] T. Kinoshita *et al.*, "Fabrication of vertical Schottky barrier diodes on n-type freestanding AlN substrates grown by hydride vapor phase epitaxy," *Appl. Phys. Express*, vol. 8, no. 6, p. 061003, May 2015, doi: 10.7567/APEX.8.061003.

[18] F. Iucolano, F. Roccaforte, F. Giannazzo, and V. Raineri, "Barrier inhomogeneity and electrical properties of Pt/GaN Schottky contacts," *J. Appl. Phys.*, vol. 102, no. 11, p. 113701, Dec. 2007, doi: 10.1063/1.2817647.

[19] Y. Ohno, T. Nakao, S. Kishimoto, K. Maezawa, and T. Mizutani, "Effects of surface passivation on breakdown of AlGaN/GaN high-electron-mobility transistors," *Appl. Phys. Lett.*, vol. 84, no. 12, pp. 2184–2186, Mar. 2004, doi: 10.1063/1.1687983.

[20] C. I. Wu and A. Kahn, "Electronic states at aluminum nitride (0001)-1×1 surfaces," *Appl. Phys. Lett.*, vol. 74, no. 4, pp. 546–548, Jan. 1999, doi: 10.1063/1.123140.

[21] M. S. Miao, A. Janotti, and C. G. Van de Walle, "Reconstructions and origin of surface states on AlN polar and nonpolar surfaces," *Phys. Rev. B, Condens. Matter*, vol. 80, p. 155319, Oct. 2009, doi: 10.1103/PhysRevB.80.155319.

[22] P. Reddy *et al.*, "The effect of polarity and surface states on the Fermi level at III-nitride surfaces," *J. Appl. Phys.*, vol. 116, no. 12, p. 123701, Sep. 2014, doi: 10.1063/1.4896377.

[23] B. M. Green, K. K. Chu, E. M. Chumbes, J. A. Smart, J. R. Shealy, and L. F. Eastman, "The effect of surface passivation on the microwave characteristics of undoped AlGaN/GaN HEMTs," *IEEE Electron Device Lett.*, vol. 21, no. 6, pp. 268–270, Jun. 2000.

[24] J. P. Ibbetson, P. T. Fini, K. D. Ness, S. P. DenBaars, J. S. Speck, and U. K. Mishra, "Polarization effects, surface states, and the source of electrons in AlGaN/GaN heterostructure field effect transistors," *Appl. Phys. Lett.*, vol. 77, no. 2, pp. 250–252, Jul. 2000, doi: 10.1063/1.126940.

[25] M. Dutta, F. Koeck, R. Hathwar, S. Goodnick, R. Nemanich, and S. Chowdhury, "Demonstration of diamond-based Schottky p-i-n diode with blocking voltage > 500 V," *IEEE Electron Device Lett.*, vol. 37, no. 9, pp. 1170–1173, Sep. 2016, doi: 10.1109/LED.2016.2592500.

[26] H. Fu, X. Huang, H. Chen, Z. Lu, I. Baranowski, and Y. Zhao, "Ultra-low turn-on voltage and on-resistance vertical GaN-on-GaN Schottky power diodes with high mobility double drift layers," *Appl. Phys. Lett.*, vol. 111, no. 15, Oct. 2017, Art. no. 152102, doi: 10.1063/1.4993201.

[27] S. J. Pearton, R. Deist, F. Ren, L. Liu, A. Y. Polyakov, and J. Kim, "Review of radiation damage in GaN-based materials and devices," *J. Vac. Sci. Technol. A, Vac. Surf. Films*, vol. 31, no. 5, Apr. 2013, Art. no. 050801.

[28] K. H. Chow *et al.*, "Intrinsic defects in GaN. I. Ga sublattice defects observed by optical detection of electron paramagnetic resonance," *Phys. Rev. B, Condens. Matter*, vol. 69, no. 4, p. 045207, Jan. 2004.

[29] A. Y. Polyakov *et al.*, "Neutron transmutation doping effects in GaN," *J. Vac. Sci. Technol. B, Microelectron. Process. Phenom.*, vol. 28, no. 3, pp. 608–612, May 2010.

[30] A. P. Karmarkar *et al.*, "Proton-induced damage in gallium nitride-based Schottky diodes," *IEEE Trans. Nucl. Sci.*, vol. 52, no. 6, pp. 2239–2244, Dec. 2005.